

Single-quasiparticle stability and quasiparticle-pair decay in $\text{YBa}_2\text{Cu}_3\text{O}_{6.5}$ (Ortho II)

N. Gedik,* P. Blake, R.C. Spitzer, and J. Orenstein

Physics Department, University of California, Berkeley and

Materials Science Division, Lawrence Berkeley National Laboratory, Berkeley, CA 94720

Ruixing Liang, D.A. Bonn, and W.N. Hardy

*Department of Physics and Astronomy, University of British Columbia,
Vancouver, British Columbia, Canada V6T 1Z1*

(Dated: July 25, 2018)

We report results and analysis of time-resolved photoinduced reflectivity experiments on the cuprate superconductor $\text{YBa}_2\text{Cu}_3\text{O}_{6.5}$. The sample, which has $T_c=45$ K, was characterized by a high degree of purity and Ortho II ordering. The change in reflectivity ΔR was induced and probed using pulses of 100 femtosecond duration and photon energy 1.55 eV from a Ti:Sapphire laser. We provide a detailed picture of the decay rate γ of ΔR as a function of temperature T and pump intensity I . At low T , γ decreases linearly with decreasing I , extrapolating to nearly zero in the limit that I tends to zero. At higher temperature γ has the same linear dependence, but with nonzero limit as $I \rightarrow 0$. In the interpretation of these results we assume that ΔR is proportional to the nonequilibrium quasiparticle density created by the laser. From an analysis of the γ vs. I we estimate β , the coefficient of proportionality relating the quasiparticle decay rate to the density. The intercept of γ vs. I yields the thermal equilibrium quasiparticle decay rate. In a discussion section, we argue that the quasiparticles induced by the laser occupy primarily states near the antinodal regions of the Brillouin zone. We explain the divergence of the lifetime of these particles as T and I both tend to zero as a consequence of momentum and energy conservation in electron-electron scattering. Next, we discuss the significance of the measured value of β , which is $\approx 0.1 \text{ cm}^2\text{s}^{-1}$. We point out that the natural unit for β in a two-dimensional superconductor is \hbar/m^* , and define a dimensionless constant C such that $\beta \equiv C\hbar/m^*$. If the decay process is one in which quasiparticles return to the condensate with emission of a phonon, then C is a measure of the electron-phonon interaction. Alternatively, expressing the marginal Fermi liquid scattering in the normal state in terms of an effective β implies $C = 1/\pi$, which is in excellent agreement with the experimentally determined value in the superconducting state.

PACS numbers: 74.25.Gz, 78.47.+p

I. INTRODUCTION

A special property of the cuprate superconductors is that the energy required for the creation of a quasiparticle depends on the direction of its momentum [1]. The creation energy is zero for momenta in the 'nodal' direction, oriented at 45° relative to the Cu-O bond. The most energetically expensive quasiparticles are the 'antinodal' ones, whose momenta are nearly parallel to the bond. Because they feel the pairing interaction most strongly, their properties may hold the key to high- T_c superconductivity. Unfortunately, their tendency to form strong pairs makes them difficult to study. In thermal equilibrium the population of quasiparticles is overwhelmingly dominated by the low energy nodal ones. As a result, transport measurements performed in equilibrium, such as microwave [2] and thermal [3] conductivity, are insensitive to antinodal quasiparticles.

A potentially powerful approach to studying the interactions of antinodal quasiparticles at low temperature is

to create a nonthermal population by external excitation. By probing the relaxation of the nonthermal population to the ground state, one may hope to learn about interactions between quasiparticles that would not normally be present at low temperature. Time-resolved optical techniques are ideally suited to creating a nonequilibrium density of quasiparticles and measuring their subsequent relaxation. These techniques are based on mode-locked lasers that produce pulses of 10-100 fs duration with a wide range of energy per pulse, center wavelength, and repetition rate. Such measurements are performed in a 'pump-probe' mode in which a beam of pulses is split in two. The pump pulse creates the nonequilibrium state while the probe pulse senses the change in the optical response of the medium due to the nonequilibrium population. The time delay between the two pulses is controlled continuously and accurately by varying the optical path length difference between the two beams. Measuring the transmission or reflection of the probe as a function of time delay gives information about the return to equilibrium after the pulsed excitation.

There have been several time-resolved optical measurements performed on the $\text{YBa}_2\text{Cu}_3\text{O}_{7-x}$ (YBCO) system of cuprate superconductors. The earliest work [4, 5, 6, 7]

*Electronic address: gedik@socrates.berkeley.edu

reported the change in the reflectivity (ΔR) of a 1.5 eV probe due to photoexcitation at the same energy. The measurements showed that in the normal state ΔR is small and decays very rapidly. Upon cooling below T_c , ΔR increases rapidly, and its decay rate decreases. These results suggested that carrier thermalization and/or recombination proceed rapidly in the normal state, but are strongly impeded by the opening of the superconducting gap.

Subsequent measurements provided a more detailed picture of the magnitude and decay rate of ΔR as a function of carrier concentration [8]. In underdoped samples ΔR is readily detectable in the normal state. The decay rate slows with cooling, suggesting a correlation between the relaxation rate of the nonequilibrium state and the appearance of the pseudogap. It was reported that the relaxation time is insensitive to T in the superconducting state, with the exception of a peak near T_c . The results were interpreted in terms of an excited state in which quasiparticles and phonons rapidly reach quasiequilibrium. The decay rate was conjectured to reflect the thermalization of nonequilibrium phonons.

Recently, measurements of ΔR at 1.5 eV were reported on an untwinned single crystal of $\text{YBa}_2\text{Cu}_3\text{O}_{6.5}$ Ortho II [9]. (The designation Ortho II refers to the macroscopic ordering of the atomic layer containing the Cu-O chains. In the Ortho II phase the chains alternate between fully occupied, and entirely unoccupied, by O atoms). In these measurements the range of pump intensity was extended to nearly two orders of magnitude smaller than used in earlier measurements. It was shown that while the T dependence of the decay rate is weak when the intensity, I , is large, it becomes extremely strong as I is reduced. In fact, the decay rate appeared to vanish as T and I both tend to zero. It was suggested that the strong I dependence of the decay rate is not consistent with a picture in which the quasiparticles and phonons reach quasiequilibrium and an alternate mechanism involving the pairwise scattering of quasiparticles was suggested.

In this paper, we present further measurements and analysis of time-resolved photoinduced reflectivity in YBCO Ortho II. The experimental apparatus and sample characterization are described in Section II. In Section III we introduce the Rothwarf-Taylor (RT) equations, which provide a phenomenological framework for interpreting nonequilibrium dynamics in superconductors. Section IV presents measurements of the decay of the photoinduced reflectivity as a function of time, temperature, and pump beam intensity. The essential experimental finding, as in Ref. [9], is that the characteristic decay time diverges as both T and I approach zero. However, we present several results beyond those already reported. We present and analyze the time dependence of the transient reflectivity, showing that it is described well by the pairwise scattering of quasiparticles. Second, we report improved measurements of the asymptotic value of the decay rate in the limit that I goes to zero. According to the RT equations, the low-intensity limit is a direct measure of γ_{th} ,

the quasiparticle recombination rate in thermal equilibrium. Through improvements in sensitivity we were able to measure γ_{th} with more than one order of magnitude greater precision than previously. Finally, in Section V we present analysis and interpretation of the experimental results. We argue that the quasiparticles that give rise to ΔR are antinodal in character and interpret the decay rate as a measure of the strength of antinodal quasiparticle interactions.

II. EXPERIMENTAL METHODS

Pump and probe measurements were performed on a mechanically detwinned single crystal of $\text{YBa}_2\text{Cu}_3\text{O}_{6.5}$ with $T_c=45$ K. The sample was grown in a BaZrO_3 crucible, which yields material with purity at the 0.99995 level. The high purity allows the development of very long correlation lengths ($\xi_a = 148\text{\AA}$, $\xi_b = 430\text{\AA}$, $\xi_c = 58\text{\AA}$) of Ortho II order [10], in which the charge reservoir layer consists of alternating filled and empty copper oxygen chains. Together with $\text{YBa}_2\text{Cu}_4\text{O}_8$, it is one of two underdoped cuprate superconductors in which doping does not introduce disorder. The relative lack of disorder is reflected in the low temperature transport properties, which indicate quasiparticle scattering times in excess of 30 ps [11].

In our experiments, the pump and probe beams were produced by a mode-locked Ti:Sapphire laser. The pulses have duration 100 fs, repetition rate 12 ns, and center wavelength 800 nm. Both pump and probe beams were focused onto the sample with a 20 cm focal length lens, yielding a spot size of 75 μm diameter. The reflected probe beam was focused onto a Si photodiode detector.

A double modulation scheme was used to optimize sensitivity to small changes in the power of the reflected probe beam. In order to minimize the noise from the Si photodiode detector, a photoelastic modulator was used to modulate the amplitude of the pump beam at 100 KHz. In addition, a galvanometer-mounted mirror varied the path-length difference between pump and probe beams at a frequency of 40 Hz. This yields a rapid scan of the time delay between pump and probe, which helps to suppress noise due to 1/f fluctuations of the probe beam power. In order to demodulate and extract ΔR as a function of time delay, the output of the Si photodiode was sent to a lock-in amplifier for phase-sensitive detection of the 100 KHz component. The output of the lock-in was then sent to a digital oscilloscope whose time base was triggered synchronously to the oscillating mirror. With the oscilloscope in averaging mode, a minimum detectable $\Delta R/R$ of $\approx 10^{-7}$ could be achieved after approximately 10 minutes of accumulation time.

In this study, we focused on the decay rate of ΔR immediately following the pulsed excitation, or $\gamma(0)$. For most of the measurements, we determined $\gamma(0)$ by fitting $\Delta R(t)$ at small time delays by a decaying exponential. However, special considerations arose in measure-

ments of $\gamma(0)$ at very low pump power. As described in succeeding sections, $\gamma(0)$ decreases as the pump intensity is lowered. At low temperatures, the decay rate decreases to the extent that the change in ΔR over the 25 ps time delay range produced by the oscillating mirror is extremely small. To measure $\gamma(0)$ in this regime, we switched to a detection scheme that probes directly the derivative of ΔR with respect to time delay. The signal from the first lock-in was sent to a second lock-in, rather than the digital oscilloscope, for phase-sensitive detection at the frequency of the oscillating mirror. When the oscillating time delay is less than the decay time of ΔR , the output of the second lock-in is proportional to the derivative $d\Delta R/dt$. In this mode of data acquisition we vary the pump-probe delay by a conventional system of a retroreflector mounted on a translation stage.

When measured at low pump intensity, $\gamma(0)$ is remarkably sensitive to T , decreasing about an order of magnitude between 15 and 10 K, for example. The extreme sensitivity to temperature suggests that laser heating can introduce significant error in determining the T -dependence of $\gamma(0)$. (By laser heating we refer to the steady-state increase in sample temperature due to the time-averaged laser power). For the experiments described above, the pump intensity was lowered below the intensity of the probe. In this regime, the probe beam is responsible for heating the photoexcited region. At low temperature we can readily observe that $\gamma(0)$ varies as the probe intensity, and consequently the sample temperature, is varied. The obvious remedy of reducing the probe power has the drawback that the ΔR signal soon disappears below the detector noise level.

Empirically, we found that the optimal compromise between signal-to-noise ratio and laser heating is obtained at a probe power of approximately 1.2 mW. At this power level $\gamma(0)$ can be measured, yet the induced temperature change is significantly less than the bath temperature. Determining the dependence of $\gamma(0)$ on T at this power level requires that we know the temperature of the photoexcited region of the sample. Unfortunately it is extremely difficult to measure, with the required accuracy, the temperature of the sample directly under the focal spot.

Because of this difficulty, we have performed a numerical simulation of the thermal diffusion equation to estimate the laser-induced temperature change. We input to this simulation a realistic model for the thermal properties of the sample and its coupling to the bath. In the experiment, the sample is attached to a sapphire plate using thermal grease. After mounting, the thickness of the grease layer is determined using an optical microscope. The input parameters to the numerical simulation are the thicknesses of the sample and grease layer, as well as their temperature dependent thermal conductivities [12, 13]. Figure 1 shows the temperature of the photoexcited region as a function of the bath temperature, as determined by finite-element analysis of the diffusion equation. In the simulation, the laser power is 1.2

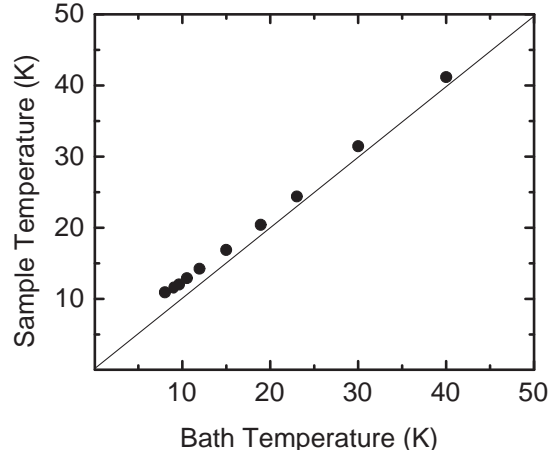


FIG. 1: Temperature of the photoexcited region of the sample as a function of the bath temperature, as determined by numerical simulation.

mW, focused to a spot of diameter $75 \mu\text{m}$. The thickness of the sample and thermal grease were $20 \mu\text{m}$ and $5 \mu\text{m}$, respectively. In the subsequent analysis of the low-pump intensity data, we used the calculated temperature, rather than the temperature of the thermal bath.

III. BACKGROUND: ROTHWART-TAYLOR EQUATIONS AND THE PHONON-BOTTLENECK

In this section we introduce the Rothwarf-Taylor [14] equations, which provide a successful phenomenological framework for understanding nonequilibrium dynamics in superconductors [15]. The RT equations are a pair of rate equations that describe a system of superconducting quasiparticles coupled to phonons. In the RT phenomenology the excited state is characterized by number densities rather than nonequilibrium energy distribution functions. This drastic simplification is justified in s-wave superconductors because quasiparticles rapidly thermalize to a narrow range of energy just above the gap. In d-wave superconductors the time evolution of the quasiparticle distribution function may be more complicated. In spite of this, we have found that the RT equations provide an excellent description of the dynamics of YBCO Ortho II after pulsed photoexcitation. In the final section we comment on the underlying reasons for the applicability of the RT approach.

In this work we write the RT equations in the following form,

$$\dot{n} = I_{qp} + 2N\gamma_{pc} - \beta n^2 \quad (1)$$

$$\dot{N} = I_{ph} + \beta n^2/2 - \gamma_{pc}N - (N - N_{eq})\gamma_{esc} \quad (2)$$

where n , and N , are the number densities of gap energy quasiparticles and phonons, respectively. The right hand side of Eq. 1 expresses the difference between the rates of quasiparticle creation and annihilation. I_{qp} is the external generation rate and $2N\gamma_{pc}$ is the rate of pair creation *via* annihilation of gap energy phonons. The quasiparticle annihilation rate βn^2 varies quadratically with density because recombination is a two-particle scattering event. In Eq. 2 the time rate of change of the phonon density is given by the external phonon creation rate and the same recombination and pair creation terms (with opposite signs) as in Eq. 1. The parameter γ_{esc} , which appears in the last term in Eq. 2, is the rate at which a gap energy phonon decays into below-gap energy phonons that cannot regenerate a quasiparticle pair. Typically, $\gamma_{esc} \ll \gamma_{pc}$, in which case a gap energy phonon is far more likely to regenerate a quasiparticle pair than to decay into the bath. Although the escape process is relatively slow, it is essential for the ultimate return of the coupled system to equilibrium.

In the present paper, we are concerned with the evolution of the system following pulsed excitation, in which case there are two characteristic time regimes. For delay times t such that $t \ll \gamma_{pc}^{-1}$, the quasiparticles and phonons have not yet reached quasiequilibrium. In this regime the quasiparticle population decays at the density dependent rate βn . For $t \gg \gamma_{pc}^{-1}$ the exchange of energy between the phonons and quasiparticles has brought the two populations into quasiequilibrium. In this regime N and n both decay at the much slower rate γ_{esc} . The decay of the quasiparticle population has become slow and independent of density, despite the fact that the rate of quasiparticle scattering may be rapid and density dependent. The limit on the decay of the nonequilibrium quasiparticle density imposed by the quasiequilibrium with the phonons is termed the phonon bottleneck.

IV. EXPERIMENTAL RESULTS

A. Intensity dependence at low temperature

The decay rate of the photoinduced reflectivity in YBCO Ortho II depends strongly on both the temperature, T , and the pump intensity, I . Fig. 1 illustrates the decrease of the decay rate with decreasing I at a fixed $T=9$ K. Each curve, measured using a different I in the range from 2 to 25 mW, has been normalized to the same value at $t = 0$ to illustrate the variation in decay rate. Although the decay rate continues to decrease as I is lowered below 2 mW, these curves are not shown because their noise fluctuations obscure the higher intensity curves. We discuss the decay rate at very low pump intensity in more detail in Section IV.C.

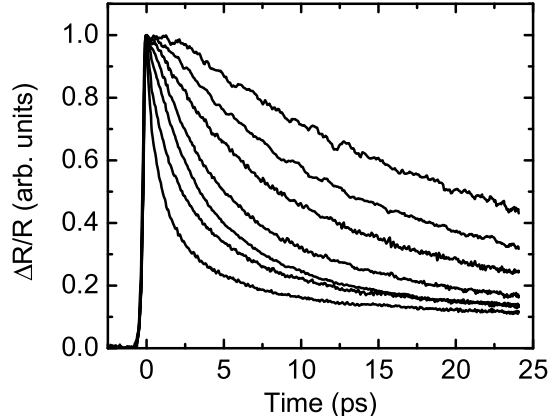


FIG. 2: $\Delta R/R$ at $T=9$ K as a function of time following pulse excitation, for several pump intensities. All curves were normalized to the same value at delay time zero to illustrate the variation in initial decay rate. The most rapid decay is seen at the highest pump intensity, corresponding to 25 mW of laser power focused to spot of diameter $75\mu\text{m}$. The decay becomes systematically slower as the intensity is reduced by factors 0.69, 0.44, 0.24, 0.15, 0.10, and 0.06.

The variation in decay rate with excitation density observed in YBCO Ortho II is highly unusual. Analogous experiments on s-wave superconductors have consistently found that the decay rate of the nonequilibrium state is independent of the quasiparticle density [15]. The lack of density dependence is understood as a manifestation of the phonon bottleneck effect. As discussed in the previous section, the bottleneck sets in when t reaches approximately γ_{pc}^{-1} . If there is no significant recombination on this time scale, that is if $\beta n \ll \gamma_{pc}$, then only density-independent bottleneck dynamics can be seen.

Within this picture, the absence of a bottleneck in YBCO Ortho II indicates that the hierarchy of pair creation and recombination rates is reversed as compared with conventional superconductors. (In Section V.D we discuss why the hierarchy of rates may be reversed in cuprate superconductors). If $\beta n \gg \gamma_{pc}$, then in the time window $t < \gamma_{pc}^{-1}$ quasiparticle recombination proceeds in the absence of the reverse process of pair creation. Measuring the decay of the quasiparticle density in this time window provides direct information about the rate of quasiparticle-quasiparticle scattering.

To test whether our measurements of YBCO Ortho II are in a pre-bottleneck regime, we have analyzed the time-dependence of the decay of ΔR . Fig. 3 is a double log plot of ΔR as a function of time delay, for several pump intensities. At the highest excitation density ΔR decays as a power law for $t > 3$ ps. With decreasing excitation density the onset of power law decay shifts to longer times. At the lowest intensity the crossover time is greater than the maximum time delay in this set of measurements, which is ~ 25 ps.

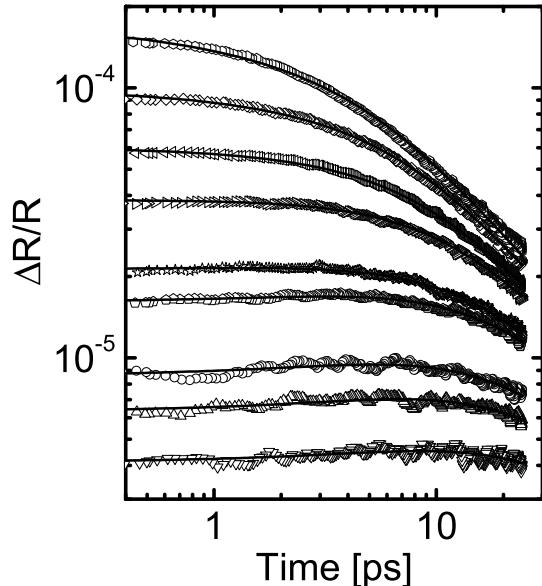


FIG. 3: $\Delta R/R$ vs. time delay at $T=9\text{K}$ plotted on a double logarithmic scale, for pump laser powers (in mW) 0.1, 0.2, 0.4, 0.6, 1.0, 1.5, 2.4, 3.8, 6.0.

We compare these curves with the predictions of the RT equations in the time regime before the onset of the phonon bottleneck. This decoupled regime corresponds to the $\gamma_{pc} \rightarrow 0$ limit. In this limit the form of the RT equations is clarified if the total quasiparticle population is written as $n_{ph} + n_{th}$, where n_{ph} and n_{th} are the photoinduced and thermal equilibrium quasiparticle density, respectively. Similarly, we define N_{ph} and N_{th} as the photoinduced and thermal equilibrium phonon populations. Detailed balance relates the thermal densities of phonons and quasiparticles such that,

$$2N_{th}\gamma_{pc} = \beta n_{th}^2. \quad (3)$$

Substituting the above relation into Eq. 1, and setting $\gamma_{pc} = 0$, yields a rate equation for n_{ph} that is independent of the phonon population,

$$\dot{n}_{ph} = I_{qp} - \beta n_{ph}^2 - 2\beta n_{th}n_{ph}. \quad (4)$$

Eq. 4 is equivalent to the rate equation applicable to nonequilibrium electrons and holes in semiconductors, and has been studied extensively in connection with photoconductivity [16]. If n_{th} vanishes as T approaches zero, then the rate equation approaches $\dot{n}_{ph} = I_{ph} - \beta n_{ph}^2$. At low T the quasiparticles obey simple second order, or bimolecular, reaction kinetics. Integration yields the decay after pulsed excitation,

$$n_{ph}(t) = \frac{n_{ph}(0)}{[1 + \beta n_{ph}(0)t]}. \quad (5)$$

Eq. 5 predicts that the excited population approaches $1/\beta t$ for $t \gg 1/\beta n_{ph}(0)$, regardless of the initial quasiparticle density. However, as is clear from Fig. 3, the measured decay curves do not obey this prediction. At long times the decay is closer to $t^{-0.8}$ than t^{-1} , and curves for different intensities do not merge to a single curve at long times.

The discrepancies described above can be traced to a complication omitted from the preceding analysis. Because the intensity of the pump beam decreases exponentially with increasing depth below the sample surface, z , the local quasiparticle density, $n_{ph}(z, t)$, is spatially nonuniform. The initial local density $n_{ph}(z, 0)$, equals $n_{ph}(0, 0)e^{-\alpha z}$, where α is the absorption coefficient at the pump wavelength. Assuming negligible diffusion of excitations in the z direction, the local excitation density decays as,

$$n_{ph}(z, t) = \frac{n_{ph}(z, 0)}{[1 + \beta n_{ph}(z, 0)t]}. \quad (6)$$

The probe beam, whose change in reflectivity measures the excited quasiparticle density, also decays exponentially in the sample. Therefore the measured reflectivity change is related to an exponentially weighted average of the nonequilibrium quasiparticle density [17],

$$\mathcal{N}(t) \equiv \alpha^{-1} \int_0^\infty dz e^{-\alpha z} n_{ph}(z, 0) / [1 + \beta n_{ph}(z, 0)t]. \quad (7)$$

Assuming that the change in reflectivity is proportional to \mathcal{N} finally yields,

$$\Delta R(t) = \frac{2\Delta R(0)}{\gamma_0 t} \left[1 - \frac{\ln(1 + \gamma_0 t)}{\gamma_0 t} \right], \quad (8)$$

where $\gamma_0 \equiv \beta n_{ph}(0, 0)$.

The solid lines in Fig. 3 indicate the best fit of Eq. 8 to the experimental data. The fit is obtained by varying $\Delta R(0)$ and γ_0 for each curve. There is excellent agreement between the data and the prediction of the bimolecular rate equation when the exponential variation of the pump and probe intensities is taken into account. The agreement suggests that for $t < 25$ ps, the phonon bottleneck is not yet established and the decay rate of ΔR is a direct measure of the quasiparticle-quasiparticle scattering rate.

From the fitting procedure we determine $\Delta R(0)$ and γ_0 for each curve. In Fig. 4 we plot γ_0 as a function of $\Delta R(0)/R$. It is evident that the characteristic decay rate increases *linearly* with the magnitude of the initial reflectivity change. The linear relationship indicates that the entire family of decay curves can be described by a single bimolecular coefficient β .

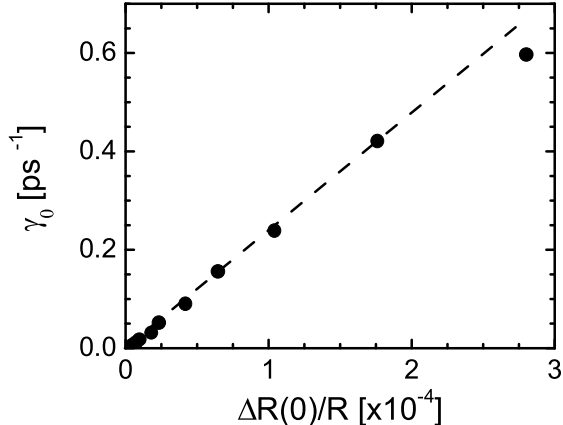


FIG. 4: The initial decay rate at the sample surface, γ_0 , as a function of the initial reflectivity change, $\Delta R(0)/R$. The dashed line emphasizes the linear dependence of initial decay rate on initial density.

B. Temperature dependence

In the previous section we showed that the decay of ΔR at low temperature can be described by the bimolecular rate equation with a single value of the scattering coefficient β . In this section we analyze the effect of raising the temperature on the rate of decay of ΔR . Fig. 5 shows a set of normalized decay curves of ΔR , measured in the temperature range from 5-70 K, induced by a pump power of 2.5 mW. The set of curves illustrates clearly that the decay rate at fixed I increases rapidly with increasing T .

To analyze the T dependence, we again consider the RT equation in the decoupled regime (Eq. 4). At nonzero T we must include the last term on the right-hand side, which was neglected previously. Physically, this term describes the rate of scattering of a photoinjected quasiparticle by a thermal equilibrium one.

We have found that the most direct way to compare the data with Eq. 4 is to focus on the initial decay rate, $\gamma(0)$, of the experimentally measured transients. Here $\gamma(0)$ is defined as the limit of the instantaneous decay rate $\gamma(t) \equiv -\dot{n}_{ph}/n_{ph}$ as t approaches zero. According to Eq. 4, $\gamma(0) = \beta [n_{ph}(0) + 2n_{th}]$. Assuming that the initial reflectivity change is proportional to $n_{ph}(0)$, a plot of $\gamma(0)$ vs. $\Delta R(0)/R$ should yield a straight line with slope proportional to β and intercept $2\beta n_{th}$.

Fig. 6 shows $\gamma(0)$ plotted as a function of $\Delta R(0)/R$ for several temperatures in the superconducting state. The data at the lowest temperature are essentially equivalent to the results presented earlier. In Fig. 4 the decay rate was determined by fitting the entire time dependence, while in Fig. 6 the decay rate is determined from the initial slope. The reason the decay rates in the two figures differ by a factor of two can be understood from Eq. 8.

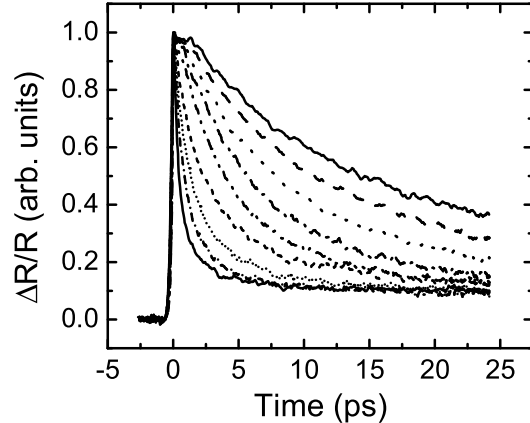


FIG. 5: $\Delta R/R$ induced by 2.5 mW of laser power, as a function of time following pulse excitation, for several temperatures in the range from 5-70 K. All curves were normalized to the same value at delay time zero to illustrate the variation in initial decay rate. The decay is most rapid at the highest temperature, and becomes systematically slower as T is reduced from 70 K to 50 K, 44 K, 28 K, 22 K, 17 K, 12 K, and 5 K.

Taking the derivative of this formula with respect to time shows that $\gamma(0) = \gamma_0/2$.

With increasing T the $\gamma(0)$ vs. $\Delta R(0)$ plots shift vertically, with little change in slope. The fact that the slope is nearly constant implies that β depends weakly, if at all, on the temperature. The increase of the intercept with T implies a rapidly increasing density of thermal equilibrium excitations. In the next section we examine the temperature dependence of the intercepts, as determined from measurements performed at very low pump and probe intensities.

Fig. 7 presents a different perspective of the decay rate as a function of temperature and intensity: $\gamma(0)$ as a function of T for three values of I . In the normal state and just below T_c the different data sets lie on the same curve, indicating that $\gamma(0)$ is independent of I . As the temperature is lowered below T_c the decay rates measured with different pump intensities begin to diverge. As the temperature tends to zero, the decay rate crosses over to a temperature independent regime, with the crossover temperature higher when the rates are measured at greater pump intensity. A consistent explanation for the T and I dependence of $\gamma(0)$ can be found in the picture of pairwise scattering involving both thermal equilibrium and photoinduced quasiparticles. The lack of intensity dependence above T_c suggests that in this regime the thermal density of quasiparticles is far larger than the photoinduced density. The strong temperature dependence above T_c suggests that n_{th} decreases with decreasing temperature in the normal state, possibly due to the opening of the pseudogap. The onset of intensity dependence at T_c may indicate that n_{th} has become

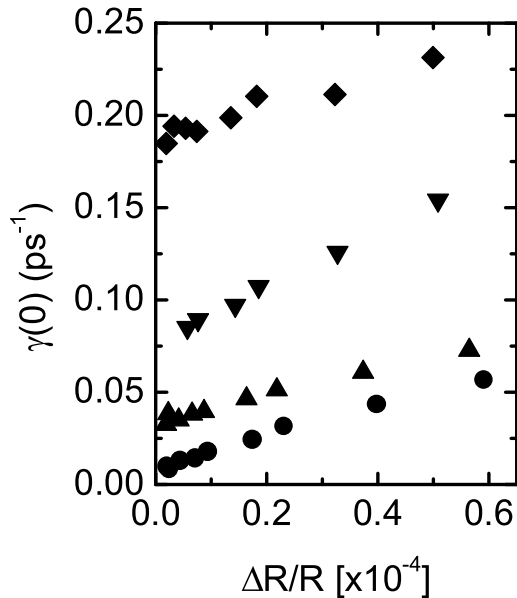


FIG. 6: Initial decay rate, $\gamma(0)$, as a function of initial reflectivity change, $\Delta R(0)/R$, for $T=12$ K, 17 K, 22 K, and 30 K. The thermal equilibrium decay rate, obtained from extrapolation of the data to zero $\Delta R(0)/R$ increases rapidly with temperature.

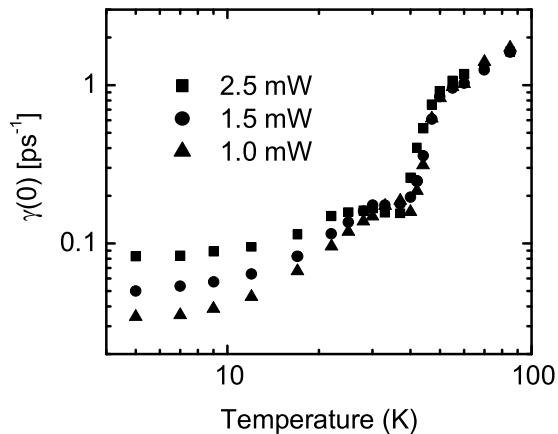


FIG. 7: Initial decay rate, $\gamma(0)$, as a function of T for three values of pump power.

comparable to n_{ph} . Alternatively, the sudden change in decay kinetics may be related to the onset of the coherence in the antinodal quasiparticle self-energy. Finally, the decay rate measured at fixed pump intensity crosses over to T -independence when n_{th} becomes much smaller than $n_{ph}(T)$. The overall behavior of $\gamma(0)$ suggests that the decay rate vanishes in the limit that both I and T go to zero.

C. Low intensity regime

In this section we focus on measurements of $\gamma(0)$ performed at the lowest laser intensities that are accessible experimentally. The motivation for studying the low-intensity regime is to measure, *via* a nonequilibrium experiment, the recombination lifetime of quasiparticles in equilibrium. In order to probe equilibrium properties, the density perturbation introduced by the laser must be small, such that $n_{ph} \ll n_{th}$. According to Eq. 4, $\gamma(0)$ approaches $2\beta n_{th}$ in this limit, which is exactly twice the thermal equilibrium recombination rate, γ_{th} .

Measuring γ_{th} accurately becomes increasingly difficult at low temperature because of the requirement that $n_{ph} \ll n_{th}$. As n_{th} decreases rapidly with decreasing T , the pump intensity must be lowered accordingly. Eventually ΔR reaches the noise floor of the experiment, which sets a limit on the smallest γ_{th} that can be measured. In principle, the signal size could be increased by raising the intensity of the probe beam. However, this inevitably leads to an increase in the average temperature of the photoexcited region compared with the bath temperature. This problem becomes increasingly severe at low temperature, where the thermal conductivity of the sample is small. For the data to be presented, the probe intensity was maintained at 1.2 mW, a value which provides the best compromise between sensitivity and heating.

At each T , we obtain $2\gamma_{th}$ from the extrapolation to zero of a linear fit to $\gamma(0)$ vs. ΔR . The temperature of the photoexcited region is determined through the numerical analysis described in Section II. Fig. 8 is a double logarithmic plot of $2\gamma_{th}$ as a function of T , showing results for both YBCO Ortho II and a thin film sample of $\text{Bi}_2\text{Sr}_2\text{CaCu}_2\text{O}_8$ (BSCCO) [18]. At the upper limit of the T range, γ_{th} is nearly identical in the two materials. However, as mentioned previously, the dependence of γ_{th} on T becomes very strong in YBCO Ortho II at low temperature. If the functional form was assumed to be a power law, then γ_{th} would approach a T^8 dependence.

We believe it to be more reasonable to assume that γ_{th} in YBCO Ortho II decreases exponentially at low temperature. To analyze this exponential dependence, we compare the data with the formula,

$$2\gamma_{th}(T) = \frac{k_B T}{\hbar} \frac{T}{T_0} \exp[-\Delta_{th}(T)/k_B T]. \quad (9)$$

We introduce a prefactor proportional to T^2 for two reasons, one theoretical and the other experimental. The theoretical reason is that $n_{th}(T)$ is predicted to vary as T^2 for a d-wave superconductor. The experimental reason is that in some samples of BSCCO γ_{th} is proportional to T^2 over the temperature range from 10 K to 40 K [18]. (The dashed line in Fig. 8 indicates a T^2 dependence). Fitting Eq. 9 to the YBCO Ortho II data yields $T_0 = 1100$ K and a temperature dependent activation energy Δ_{th} that is plotted in the inset. The

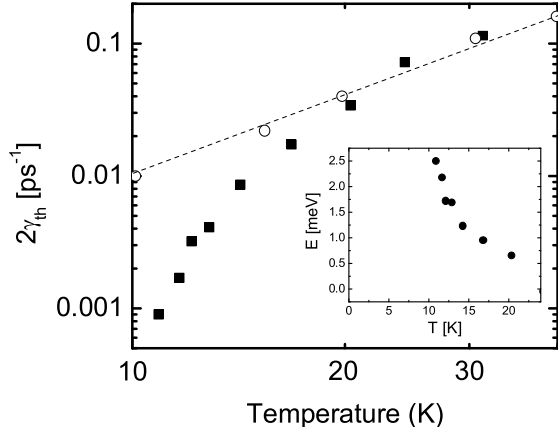


FIG. 8: Twice the thermal equilibrium recombination rate, as determined by the extrapolation of $\gamma(0)$ to zero laser power, as a function of temperature. Solid squares are results for the YBCO Ortho II sample, open circles show results obtained on a thin film sample of BSCCO with $T_c = 85$ K. The dashed line indicates a temperature dependence proportional to T^2 . The inset shows the activation energy of the recombination rate in YBCO Ortho II as determined from a fit to Eq. 9.

origin of the exponential cutoff in γ_{th} that appears in YBCO Ortho II and not in BSCCO is not understood at present. However, we note that analogous behavior is observed in the scattering rates observed by ac conductivity experiments. In the YBCO system, the mean free path increases exponentially with temperature towards a limit of several microns set by elastic processes [11]. In BSCCO the T dependence is much weaker and the limiting value is only a few hundred \AA [19]. It is possible that momentum conservation imposes constraints on the rate of quasiparticle-quasiparticle scattering in the cleaner YBCO system. These constraints may dictate that only Umklapp processes are allowed at low T , leading to an exponential T dependence [20, 21].

V. DISCUSSION

In analyzing the experimental data presented above, we begin (in Section V.A) with the most basic question: what type of excitation is probed by transient reflectivity experiments performed on the cuprate superconductors? We argue that these excitations are quasiparticles that occupy states close to the antinodal regions of the Brillouin zone. In Sections V.B and V.C we turn to a quantitative analysis of the decay rate of the photoexcited state. Section V.B focuses on our observation that the lifetime of a photoinjected quasiparticle diverges in the limit that T and I both tend to zero. We show theoretically that the constraints of momentum and energy conservation prevent thermalization of antinodal quasiparticles toward the nodes. In Section V.C we estimate

the magnitude of the recombination coefficient β from the experimental data, and discuss its theoretical interpretation. Finally, in Section V.D, we comment on possible reasons for the absence of a phonon bottleneck in the decay of the photoexcited state.

A. What types of excitations are probed?

As a first guess, one might imagine that the photoinduced quasiparticles occupy states near the nodes, as these are the lowest energy excitations. This intuition is consistent with the generally accepted picture of the quasiparticle distribution function in the nonequilibrium state. In this picture the nonequilibrium quasiparticles rapidly adopt a Fermi-Dirac distribution, but with a chemical potential, and temperature, μ^* , and T^* , respectively, that are larger than their values in thermal equilibrium [22, 23]. In a d-wave superconductor this distribution describes a population of quasiparticles that is dominated by states near the nodes ('nodal' quasiparticles). The occupation of states with energy greater than $\max(\mu^*, T^*)$ is exponentially small.

On the other hand, the experimental evidence suggests that the photoexcited state is not a degenerate gas of nodal quasiparticles. Three observations, in particular, lead us to this conclusion:

(1) *The diffusion coefficient of photoinjected quasiparticles is at least two orders of magnitude smaller than the diffusion coefficient of nodal quasiparticles* [24]. The diffusive propagation of nonequilibrium quasiparticles in YBCO Ortho II was recently measured by the transient grating technique. Values for the diffusion coefficient of $20 \text{ cm}^2/\text{s}$ and $24 \text{ cm}^2/\text{s}$ were determined for motion along the **a** and **b** crystalline axes, respectively. This may be compared with a nodal quasiparticle diffusion coefficient of $\approx 6000 \text{ cm}^2/\text{s}$ as determined from microwave spectroscopy on the same sample [11].

(2) *The reduction in the condensate spectral weight depends linearly on the pump intensity.* Information about the photoinduced reduction of condensate spectral weight comes from visible pump-terahertz probe experiments [25, 26]. At frequencies $\sim 1 \text{ THz}$, the optical conductivity $\sigma(\omega)$ is dominated by its imaginary part, σ_2 , which is proportional to the condensate density. Following photoexcitation at 1.5 eV , σ_2 drops rapidly as the condensate density is diminished. At intensities below the saturation level, the loss of condensate density is a linear function of the energy deposited in the photoexcited volume.

The linear reduction of condensate density with pump energy is inconsistent with the physics of nodal quasiparticles. This point can be illustrated by considering the temperature dependence of the superfluid density, ρ_s . Nodal quasiparticles are responsible for the linear in T decrease of ρ_s observed in clean cuprate superconductors [27]. However, the energy stored in the nodal quasiparticle gas increases not as T , but as T^3 . Therefore the reduction in ρ_s due to nodal quasiparticles varies

as the one-third power of the total energy in the quasiparticle gas. We would expect such a strongly sublinear relationship for a degenerate gas of nonequilibrium nodal quasiparticles as well.

(3) *Far-IR measurements of the photoexcited state show that the optical spectral weight that is removed from the condensate by photoexcitation shifts to energies on the order of 50-100 meV, or several times the value of the maximum gap* [28]. As discussed above, thermal excitation of nodal quasiparticles does indeed remove spectral weight from the condensate. However, the spectral weight shifts to a very narrow ($<30\mu\text{eV}$) Drude peak centered on $\omega = 0$. In contrast, the spectral weight removed from the condensate by photoexcitation shifts to frequencies that are ≈ 1000 times higher than the width of the nodal quasiparticle Drude peak. This is further evidence against a degenerate gas of nodal quasiparticles.

On the basis of the preceding arguments, we conclude that nodal quasiparticles do not dominate the population of quasiparticles created by photoexcitation. In other words, the quasiparticle distribution in the photoexcited state cannot be described as a Fermi-Dirac function with effective parameters μ^* and T^* . The experiments are more consistent with a distribution function that is peaked at an energy above the chemical potential. Such a distribution can arise if it is not possible to scatter into the nodal states during the lifetime of the photoexcited state. In Section 5.2 we show that the constraints of energy and momentum conservation severely restrict the rate at which hot quasiparticles scatter into states near the nodes.

B. Stability of an isolated photoexcited particle

In section V.A, we argued that the quasiparticle distribution function in the photoexcited state peaks at an energy above the chemical potential and therefore is not of the Fermi-Dirac form. Such a nonequilibrium distribution can arise if quasiparticles cannot scatter into nodal states during the lifetime of the photoexcited state. However, we have also shown that this lifetime can be very long, reaching ~ 0.6 ns at the lowest temperature and intensity accessible experimentally. By comparison a 30 meV excitation in a Fermi liquid (with Fermi energy ~ 1 eV) would decay into electron-hole pairs in ~ 3 ps. In the following we describe how the relative stability of a quasiparticle in a d-wave superconductor can arise from the severely restricted phase space for decay.

In a Fermi liquid, quasiparticles readily decay into particle-hole pairs because energy and momentum can be conserved in the process. However, the kinematic constraints are much more severe in the case of a d-wave superconductor. Consider the momentum-resolved particle-hole excitation spectrum in the two cases. In the Fermi liquid the particle-hole spectrum forms a broad continuum that extends from zero wavevector to twice k_F , even as the pair energy tends to zero.

The d-wave superconductor differs from the Fermi liquid in that the Fermi contour shrinks to four nodal points. As a consequence, the pair excitation spectrum is much more localized in momentum space. Fig. 9 illustrates the momentum-resolved pair excitation spectrum of a d-wave superconductor. Each plot is a color-scale depiction of the density of two-particle excitations of a given energy in the first Brillouin zone. The spectra were calculated using a parameterization of the quasiparticle dispersion obtained by Norman [29] from a fit to ARPES data. At very low energies, the pair spectrum is localized near nine discrete wavevectors that represent the creation of particles at the nodes. As the energy of the pair increases, the locus of possible wavevectors spreads out. However, for energies that are less than Δ_0 , the allowed momenta remain clustered near the nine zero-energy wavevectors.

In order for a single quasiparticle to scatter and emit a pair, its change in energy and momentum, $\Delta\epsilon$ and Δk , must match that of the pair, ϵ_{pair} and k_{pair} . The constraints imposed by this condition are illustrated in the diagrams shown in Fig. 10, which describe the possible decay events of a hot quasiparticle. For this example we have chosen a quasiparticle with energy 40 meV and momentum on the Fermi contour of the normal state. Each diagram corresponds to a fixed energy transfer in the scattering event. The color scale indicates the location of allowed values of Δk and k_{pair} at the transfer energy. A scattering event is kinematically allowed only at momentum transfers where the two sets of wavevectors overlap.

Fig. 10 illustrates how kinematics prevent the inelastic scattering of the hot quasiparticle. For example, consider the scattering events with the largest possible energy change, 40 meV. To give up all its energy the hot quasiparticle must scatter to one of the nodes, thus there are only four allowed values of Δk . (The four points are not visible in Fig. 10(a)). One of these four wavevectors just touches the perimeter of the elliptical region of pair wavevectors, which indicates an allowed scattering event. In this scattering event the hot quasiparticle scatters to the node, with the simultaneous creation of a quasihole at the node and a quasiparticle at the energy and momentum of the hot quasiparticle. This exchange process, although kinematically allowed, does not lead to a change in the particle distribution function.

If the hot quasiparticle does not lose all of its energy, there are more choices for the final momentum. The locus of allowed Δk expands, becoming visible as arcs in panels (b) through (e) of Fig. 10. However, as the arcs expand the locus of pair creation wavevectors shrinks. Fig. 10 shows that the region of allowed k_{pair} shrinks faster than the expansion of allowed Δk , so that the two regions fail to overlap at any energy transfer less than the energy of the hot quasiparticle. The absence of overlap demonstrates that the thermalization of the hot quasiparticle is forbidden because of kinematic constraints. Recently, Howell et al. [21] reached a similar conclusion based on an analytical, rather than numerical, approach.

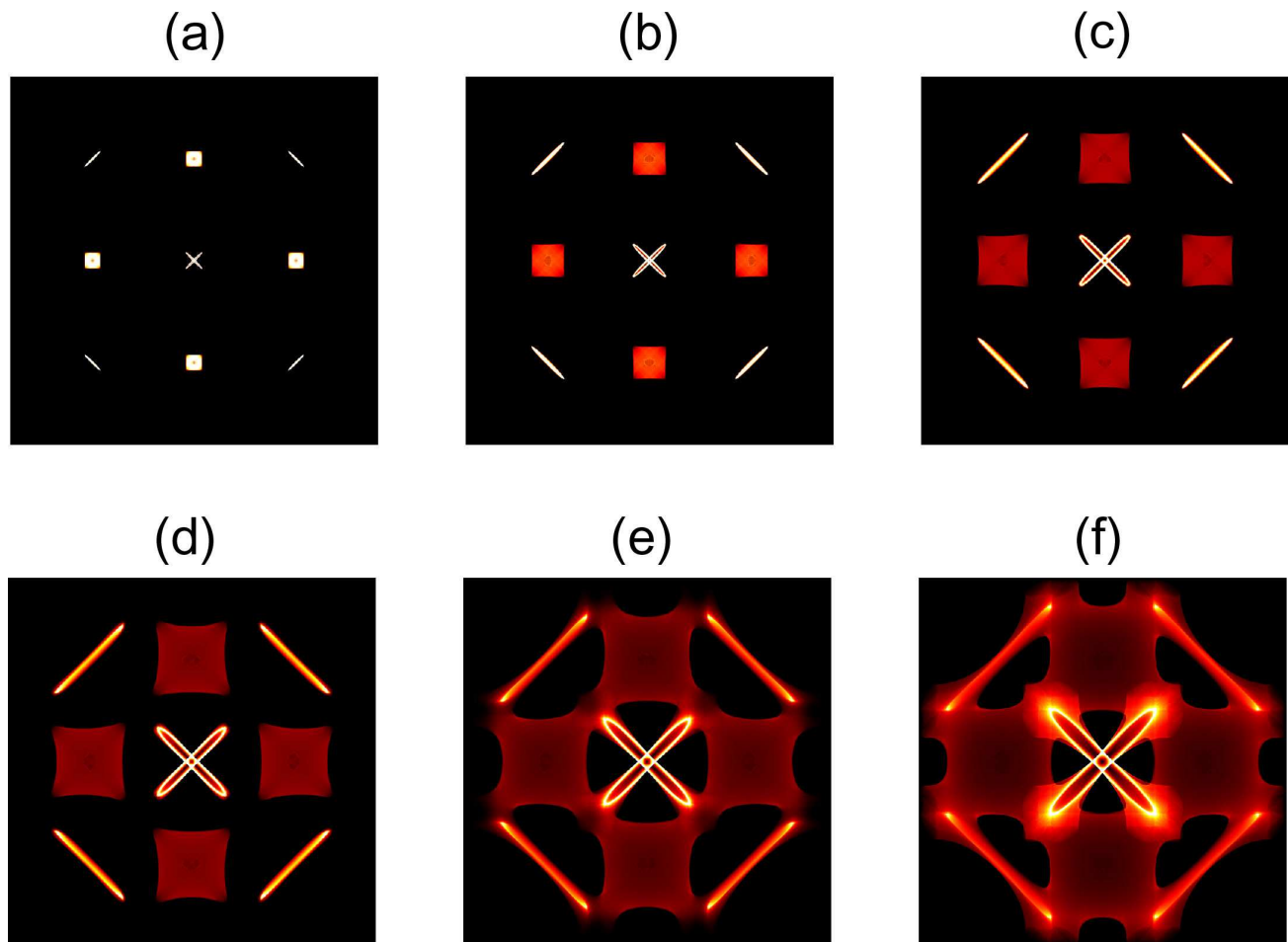


FIG. 9: Color scale depiction of quasiparticle pair momenta in the first Brillouin zone for different values of the pair energy; (a) 10 meV, (b) 20 meV, (c) 30 meV, (d) 40 meV, (e) 50 meV, and (f) 60 meV.

The kinematic constraints in this example are specific to quasiparticles near the normal state Fermi contour. They are a consequence of the rapid decrease of quasiparticle velocity with increasing distance from the node. For this reason, we anticipate that not all quasiparticles of a given energy will be stable. The contours of constant quasiparticle energy are distorted ellipses centered on each of the nodes. Quasiparticles near the major axis vertex of the ellipse will be stable, as we have seen. However, the velocity for particles near the minor axis vertex is comparable the nodal quasiparticle velocity. For these quasiparticles there are no kinematic constraints to prevent rapid thermalization. Thus, we anticipate that after a short time following pulsed injection only nonequilibrium particles near the major axis vertex will survive.

C. Bimolecular recombination

1. Estimating β

In the previous section we have seen that kinematic constraints can stabilize an isolated antinodal quasiparticle. However, our experiments show that a *pair* of quasiparticles can convert to a state which no longer contributes to ΔR . We can be confident that this conversion requires two particles, and not more, because the decay rate increases linearly with density. The coefficient that relates the decay rate to the density, β , is directly related to the cross-section for inelastic scattering of two quasiparticles. Thus the magnitude of β is of fundamental importance as a measure of the coupling of quasiparticles to some other excitation of the interacting electronic system.

We turn next to estimating β from the measured dependence of the decay rate on density. Experimentally, we measure both the nonequilibrium decay rate βn_{ph} and the thermal equilibrium rate βn_{th} . To extract β from these measurements, we need to know either n_{ph}

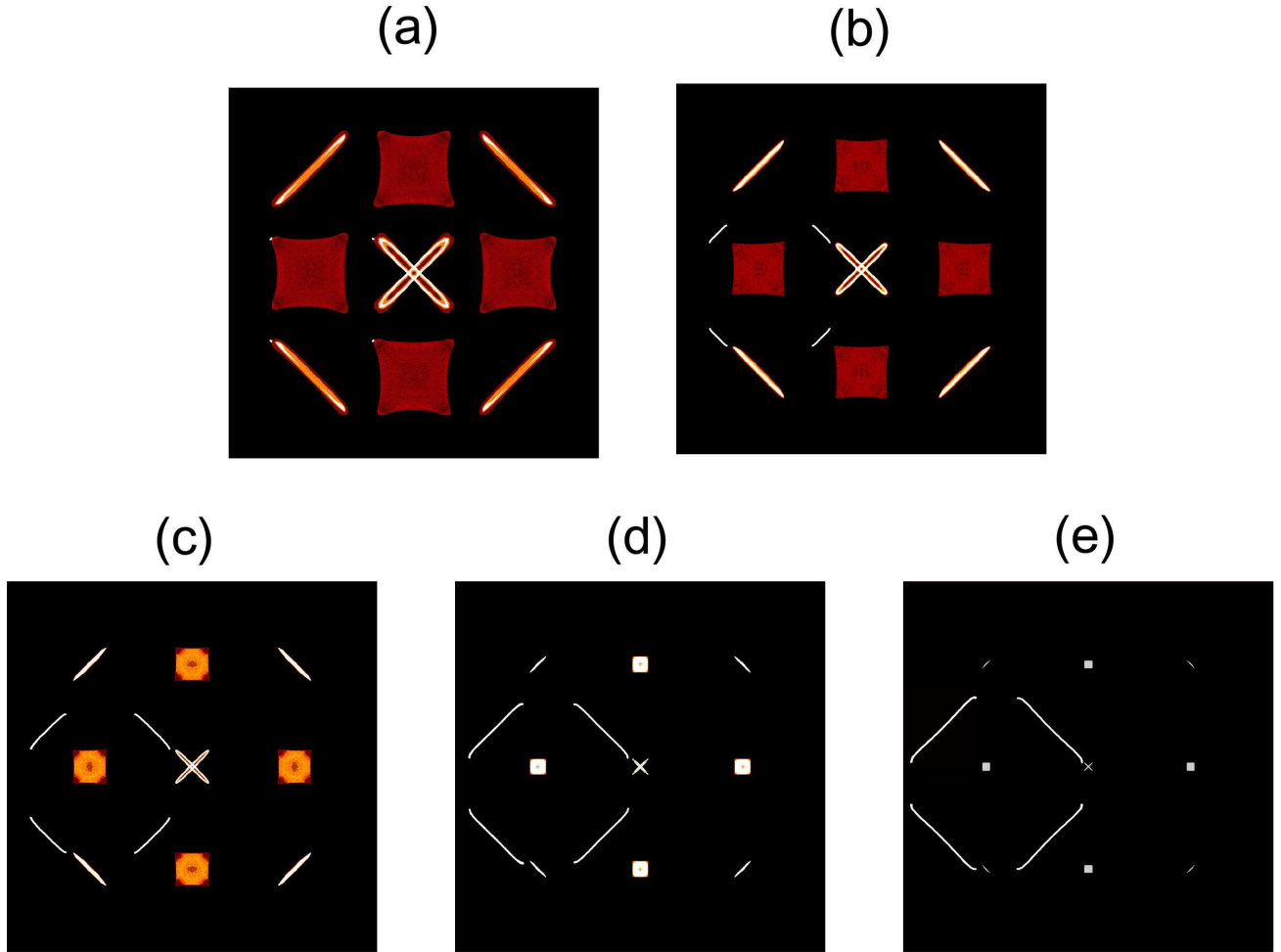


FIG. 10: Depiction of the lack of overlap between the scattering momentum Δk and the pair momentum k_{pair} . For this illustration the hot quasiparticle starts with energy 40 meV and momentum on the Fermi contour of the normal state. The arc segments in each square show the possible values of Δk for several values of the scattering energy $\Delta\epsilon$: (a) 40 meV; (b) 30 meV; (c) 20 meV; (d) 10 meV; (e) 5 meV. The color scale plot in each of the squares shows the allowed values of k_{pair} at the same energy. As the energy transfer decreases and the arc segments expand, the regions of k_{pair} shrink faster. The lack of overlap is a graphical demonstration of how momentum and energy conservation prevent thermalization of a quasiparticle near the antinodal region of the Brillouin zone.

or n_{th} . Unfortunately, neither quantity is directly determined from the data, and we need additional assumptions to estimate these quantities. To estimate n_{ph} we use energy conservation to convert from laser energy density to quasiparticle density. In the linear regime of γ vs. I a recombination rate of 10^{11} s^{-1} results from a laser energy density of 0.1 J-cm^{-3} . If photon energy is converted entirely to 40 meV quasiparticles, then their initial density is $\approx 10^{12} \text{ cm}^{-2}$, and therefore $\beta \approx 0.1 \text{ cm}^2/\text{s}$.

We can also determine β from the thermal equilibrium recombination rate as well, if we know $n_{th}(T)$. For a d-wave superconductor,

$$n_{th}(T) = \frac{\pi v_F}{6v_2} \left(\frac{k_B T}{\hbar v_F} \right)^2, \quad (10)$$

where v_F and v_2 are the nodal quasiparticle velocities

perpendicular and parallel to the Fermi contour, respectively [30]. Based on the RT equations, we would expect the thermal equilibrium decay rate to be proportional to n_{th} and thus vary with temperature as T^2 . Instead, we find experimentally that in YBCO Ortho II the limiting behavior of γ_{th} is exponential rather than power law. The unexpected exponential cutoff of the recombination rate may be related to a similar exponential cutoff seen in the momentum scattering rate as measured through microwave spectroscopy [2].

Despite the exponential cut-off of the recombination rate at low T , we can attempt to estimate β from the thermal recombination rate at higher T . Above $\approx 20 \text{ K}$, $\gamma_{th}(T)$ is not inconsistent with a quadratic dependence on temperature. In that range we found that $2\gamma_{th}(T) \approx (k_B T/\hbar)T/T_0$, with $T_0 = 1100 \text{ K}$. Assuming that $\gamma_{th} = \beta n_{th}$, and using Eq. 10 to estimate $n_{th}(T)$

(with $v_F/v_2 = 10$) we find $\beta = 0.26 \text{ cm}^2/\text{s}$. Considering the approximations and assumptions involved, this value is quite close to the one determined from the nonequilibrium recombination rate.

2. Theoretical approaches for β

Within the context of BCS theory, the process of recombination is the annihilation of a quasiparticle pair with the simultaneous emission of a gap energy phonon. The theory of the recombination rate of BCS quasiparticles was developed by Kaplan et al. [31], whose calculations assumed an isotropic s-wave gap and the breaking of momentum conservation through strong elastic scattering ('dirty limit'). Their result for the recombination rate, expressed through our definition of recombination coefficient, is $\beta = 4\pi\alpha^2(2\Delta)F(2\Delta)/\hbar N(0)$, where α , F , and N , are the electron-phonon coupling strength, density of phonon states, and density of electron states, respectively. While it is very useful to have this explicit result to compare with, we must bear in mind that the cuprate superconductors do not satisfy the assumptions upon which this calculation is based. The cuprates are 2D rather than 3D, d-wave rather than s-wave, and are in the clean, rather than the dirty, limit of elastic scattering.

We are not aware of a calculation of the phonon-mediated recombination rate applicable to the cuprate superconductors. However, in anticipation of such a calculation, we define a dimensionless constant $C \equiv \hbar\beta N(0)$, that parametrizes the electron-phonon coupling strength in the clean limit. If in addition we express the 2D electronic density of states through an effective mass m^* , then we obtain the simple formula $\beta = C\hbar/m^*$. Assuming an effective mass that is three times the free electron mass, $\hbar/m^* = 0.3 \text{ cm}^2/\text{s}$, so that $\beta = 0.1 \text{ cm}^2/\text{s}$ corresponds to $C \approx 1/3$. It is striking that C is of order unity. This suggests that, while we do not know if phonon emission is indeed the mechanism for quasiparticle recombination, we have identified \hbar/m^* as the 'natural unit' for β .

The body of experimental results on the cuprate superconductors have led many researchers to conclude that quasiparticle scattering is determined by electron-electron, rather than electron-phonon interactions. The BCS theory of recombination was adapted by Quinlan et al. [32] to the case where quasiparticle-pair energy is converted to antiferromagnetic spin fluctuations, rather than phonons. As we explain below, the results of this calculation cannot be compared directly with β . The recombination rate at low T is predicted to vary as T^3 . Therefore γ_{th} is not proportional to n_{th} , which, as we have seen, varies as T^2 . Expressed in the language of this paper, β vanishes in the limit that T goes to zero, in contrast to the T -independent value observed experimentally.

The prediction that $\gamma \propto T^3$ while $n_{th} \propto T^2$ is a reflection of the underlying Fermi liquid theory (FLT). In

FLT the normal state scattering rate varies as T^2 , while the thermal quasiparticle density varies as T . The corresponding quantities vary as one higher power of T for the d-wave superconductor because its density of states is linear in energy, rather than constant. Thus it is a general consequence of the phase space of Fermi liquids that the quasiparticle scattering rate is not simply proportional to the quasiparticle density.

It is interesting, and perhaps relevant, to recall here the celebrated fact that the high- T_c cuprates violate this central prediction of FLT. That is to say, the normal state scattering rate varies linearly, rather than quadratically, with the temperature. In this marginal Fermi liquid (MFL) [33], the scattering rate $\sim 2k_B T/\hbar$ is proportional to the quasiparticle density $N(0)k_B T$. The coefficient of proportionality, or β_{MFL} , is simply $\hbar/\pi m^*$. Evaluating this expression with $m^* = 3m_0$ yields $\beta_{MFL} = 0.1 \text{ cm}^2/\text{s}$, which is remarkably close to the experimental value. This agreement suggests that there may be a close connection between the quasiparticle scattering in the normal state and the antinodal quasiparticle recombination in the superconducting state.

D. Absence of phonon bottleneck

In the previous section we described two mechanisms for quasiparticle pair recombination. In the more familiar one, the pair is destroyed with simultaneous creation of a 2Δ phonon. In the second mechanism the pair is converted to an electronic excitation, such as an antiferromagnetic fluctuation. Both mechanisms can provide an explanation for the absence of a bottleneck. In the second mechanism, the quasiparticle pair decays to other particle-hole excitations. If the number of particles generated in the pair-destruction process is two or more, then it is highly unlikely for the reverse process to occur. The low rate for the reverse process leads to the absence of a bottleneck.

On the other hand, phonon-mediated recombination is inherently susceptible to a bottleneck because only one particle (the phonon) is created when the pair is destroyed. Following pulsed injection, the bottleneck sets in when the pair destruction and creation rates become equal, or $\beta n_{ss}^2 = 2\gamma_{pc} N_{ss}$, where n_{ss} and N_{ss} are the quasiequilibrium steady-state densities of quasiparticles and 2Δ phonons, respectively. The size of n_{ss} relative to the initial density n_0 is a measure of the strength of the bottleneck. This ratio can be calculated using conservation of energy, which implies that $2n_{ss} + N_{ss} = 2n_0$. The result is

$$\frac{n_{ss}}{n_0} = \frac{\lambda}{2} \left(\sqrt{1 + \frac{4}{\lambda}} - 1 \right), \quad (11)$$

where $\lambda \equiv 2\gamma_{pc}/\beta n_0$. The strong bottleneck regime corresponds to $\lambda \gg 1$, in which case the steady state density nearly equals the initial density, $n_{ss}/n_0 \approx 1 - 1/\lambda$. On

the other hand, if $\lambda \ll 1$ the bottleneck is practically nonexistent and the steady state density is very small, $n_{ss}/n_0 \approx \lambda^{1/2}$.

To determine whether the cuprates are in the strong or weak bottleneck regime, we must estimate the magnitude of λ . To do so we first recognize that λ must exceed a λ_{min} , obtained by setting n_0 equal to $N(0)\Delta$, the maximum quasiparticle density in the superconducting state. We can evaluate λ_{min} in the dirty s-wave case, as Kaplan et al. [31] have calculated γ_{pc} as well as β in this regime. The characteristic phonon decay rate is given by $\gamma_{pc} = 4\pi^2 N(0)\alpha^2 \Delta / \hbar N$, where N is the number density of ions. Given this phonon decay rate, we find that

$$\lambda_{min} = \frac{2\pi}{\hbar} \frac{N(0)}{NF(2\Delta)}. \quad (12)$$

The simplicity of this result is a consequence of detailed balance in the dirty-limit. Eq. 12 shows that the strength of the bottleneck is determined by the ratio of the electron density of states at the Fermi level to the phonon density of states at 2Δ . It is clear that the high- T_c cuprates can be in the weak bottleneck regime, where λ is very small, in contrast with conventional low- T_c superconductors. In the high- T_c materials the gap energy is large, and 2Δ coincides with large phonon density of states peaks associated with optic phonons. Furthermore, the density of states at the Fermi level is small compared with conventional metals. Both factors favor small λ . In contrast, in conventional superconductors phonons with energy 2Δ lie in the low-energy tail of the acoustic spectrum. Therefore the density of resonant phonon states is small. This fact, together with the large electronic density of states, place conventional superconductors in the strong bottleneck regime.

VI. SUMMARY

The most significant observation reported in this paper is the strong dependence of the decay rate of the transient reflectivity on both temperature and pump laser intensity. At low T the decay rate is a linear function of I . At low I the decay rate decreases exponentially with

decreasing T . At the lowest values of T and I probed by our experiments, the lifetime of the photoexcited state becomes extremely long, ≈ 600 ps. There is no indication that the lifetime would not continue to increase if the experiment could access lower values of T and I .

In our analysis of the data, we first addressed the nature of the excitations probed by measuring ΔR . We presented arguments that ΔR is proportional to the density of high-energy or antinodal quasiparticles created by the laser excitation. We explained theoretically why such particles, although not the lowest energy excitations, could be highly metastable at low temperature and density. The metastability is a consequence of the limited phase space for decay of high-energy quasiparticles to the nodal regions of the Brillouin zone. As the phase space restrictions rely on momentum conservation, the degree of metastability may be expected to be highly sensitive to disorder.

Having understood the stability of an isolated quasiparticle, we sought a quantitative understanding of the decay process that occurs when a pair of quasiparticles interact. We estimated the magnitude of the recombination coefficient, β , from both the T and I dependence of the decay rate. We emphasized that β is a direct measure of the strength of quasiparticle interactions. In addressing the theoretical approaches to the recombination rate, we identified \hbar/m^* as the natural unit for β in a two-dimensional superconductor. We pointed out that while recombination is assumed to be phonon-mediated in conventional superconductors, electron-electron mediated processes must be considered as well in the cuprates. In the context of phonon-mediated processes, we discussed the need to extend the work of Kaplan et al. [31] to the 2D, clean limit that is applicable to the cuprates. In the electron-electron mediated case, more work is needed to understand the underlying recombination process. As a motivating factor, we pointed out the remarkable coincidence between the normal state scattering rate and the superconducting state recombination rate. We showed that both processes have the same dependence on the quasiparticle density, which can be described by an interaction coefficient equal to $\hbar/\pi m^*$.

This work was supported by NSF-9870258, DOE-DE-AC03-76SF00098, CIAR and NSERC.

-
- [1] Z.X. Shen et al., Phys. Rev. Lett. **70**, 1553 (1993).
 - [2] A. Hosseini et al., Phys. Rev. B **60**, 1349 (1999).
 - [3] Y. Zhang et al., Phys. Rev. Lett. **86**, 890 (2001).
 - [4] S.G. Han et al., Phys. Rev. Lett. **65**, 2708 (1990).
 - [5] G.L. Eesley et al., Phys. Rev. Lett. **65**, 3445 (1990).
 - [6] J.M. Chwalek et al., Appl. Phys. Lett. **57**, 980 (1990).
 - [7] S.D. Brorson et al., Solid State Commun. **74**, 1305 (1990).
 - [8] J. Demsar et al., Europhys. Lett. **45**, 381 (1999).
 - [9] G.P. Segre et al., Phys. Rev. Lett. **88**, 137001 (2002).
 - [10] Ruixiang Liang et al., Physica C **236**, 57 (2000).
 - [11] P.J. Turner et al., Phys. Rev. Lett. **90**, 237005 (2003).
 - [12] S.J. Hagen et al., Phys. Rev. B **40**, 9389 (1989).
 - [13] M.M. Kreitman, Rev. Sci. Instr. **40**, 1562 (1969); M.M. Kreitman and J.T. Callahan, Cryogenics **10**, 155 (1970).
 - [14] A. Rothwarf and B.N. Taylor, Phys. Rev. Lett. **19**, 27 (1967).

- [15] *Nonequilibrium Superconductivity, Phonons, and Kapitza Boundaries*, Ed. K.E. Gray (Plenum Press, New York, 1981).
- [16] R.H. Bube, *Photoelectronic Properties of Semiconductors* (Cambridge University Press, 1992).
- [17] The reflectivity change is not precisely proportional to the exponentially weighted average of the quasi-particle density, see for example I.M. Fishman et al., *J. Opt. Soc. Am. B* **8**, 1880 (1981), for the exact expressions. However, we have found that the approximation used in the text is quite accurate and has the advantage of leading to analytical solutions to the bimolecular rate equation.
- [18] G.P. Segre, Ph. D. thesis, May 2001, 1980.
- [19] J. Corson et al., *Phys. Rev. Lett.* **85**, 2569 (2000).
- [20] M.B. Walker and M.F. Smith, *Phys. Rev. B* **61**, 11285 (2000).
- [21] P.C. Howell, A. Rosch, and P.J. Hirschfeld et al., [cond-mat/0307168](https://arxiv.org/abs/cond-mat/0307168)
- [22] W.H. Parker, *Phys. Rev. B* **12**, 3667 (1975).
- [23] C.S. Owen and D.J. Scalapino, *Phys. Rev. Lett.* **28**, 1559 (1972).
- [24] N. Gedik et al., *Science* **300**, 1410 (2003).
- [25] R.D. Averitt et al., *Phys. Rev. B* **63**, 140502 (2001).
- [26] M.A. Carnahan et al., in proceedings of the International Conference on Materials and Mechanisms of Superconductivity and High- T_c Superconductors (unpublished).
- [27] W.N. Hardy et al., *Phys. Rev. Lett.* **70**, 3999 (1993).
- [28] R.A. Kaindl et al., *Science* **287**, 470 (2000).
- [29] M.R. Norman, *Phys. Rev. B* **63**, 092509 (2001).
- [30] M. Chiao et al., *Phys. Rev. Lett.* **82**, 2943 (1999).
- [31] S.B. Kaplan et al., *Phys. Rev. B* **14**, 4854 (1976).
- [32] S.M. Quinlan, D.J. Scalapino, and N. Bulut, *Phys. Rev. B* **49**, 1470 (1994).
- [33] C.M. Varma et al., *Phys. Rev. Lett.* **63**, 1996 (1989).